
Article:
Oliviero, S., Giorgi, M. orcid.org/0000-0001-7763-8545 and Dall'Ara, E. orcid.org/0000-0003-1471-5077 (2018) Validation of Finite Element models of the Mouse Tibia using Digital Volume Correlation. Journal of the Mechanical Behavior of Biomedical Materials, 86. pp. 172-184. ISSN 1751-6161

https://doi.org/10.1016/j.jmbbm.2018.06.022

Journal of the Mechanical Behavior of Biomedical Materials 86 (2018) 172–184

Contents lists available at ScienceDirect

Journal of the Mechanical Behavior of Biomedical Materials

journal homepage: www.elsevier.com/locate/jmbbm

Validation of finite element models of the mouse tibia using digital volume correlation

S. Oliviero, M. Giorgi, E. Dall'Ara*

Department of Oncology and Metabolism and INSIGNEO Institute for in Silico Medicine, University of Sheffield, Pam Liversidge Building, Mappin Street, S13JD Sheffield, UK

ARTICLE INFO

Keywords:
MicroCT
MicroFE
Mouse tibia
DVC
Validation

ABSTRACT

The mouse tibia is a common site to investigate bone adaptation. Micro-Finite Element (microFE) models based on micro-Computed Tomography (microCT) images can estimate bone mechanical properties non-invasively but their outputs need to be validated with experiments. Digital Volume Correlation (DVC) can provide experimental measurements of displacements over the whole bone volume. In this study we applied DVC to validate the local predictions of microFE models of the mouse tibia in compression.

Six mouse tibiae were stepwise compressed within a microCT system. MicroCT images were acquired in four configurations with applied compression of 0.5 N (preload), 6.5 N, 13.0 N and 19.5 N. Failure load was measured after the last scan. A global DVC algorithm was applied to the microCT images in order to obtain the displacement field over the bone volume. Homogeneous, isotropic linear hexahedral microFE models were generated from the images collected in the preload configuration with boundary conditions interpolated from the DVC displacements at the extremities of the tibia. Experimental displacements from DVC and numerical predictions were compared at corresponding locations in the middle of the bone. Stiffness and strength were also estimated from each model and compared with the experimental measurements.

The magnitude of the displacement vectors predicted by microFE models was highly correlated with experimental measurements ($R^2 > 0.82$). Higher but still reasonable errors were found for the Cartesian components. The models tended to overestimate local displacements in the longitudinal direction (R^2 = 0.69–0.90, slope of the regression line = 0.50–0.97). Errors in the prediction of structural mechanical properties were 14% ± 11% for stiffness and 9% ± 9% for strength.

In conclusion, the DVC approach has been applied to the validation of microFE models of the mouse tibia. The predictions of the models for both structural and local properties have been found reasonable for most preclinical applications.

1. Introduction

Mouse models are commonly used to investigate bone remodeling and the effect of bone treatments preclinically. In particular, the mouse tibia has been previously chosen to study the bone response to *in vivo* mechanical stimulation (Birkhold et al., 2015; Holguin et al., 2014), to ovariectomy (Klinck et al., 2008; Waarsing et al., 2004), to ageing (Buie et al., 2008; Main et al., 2010) and to pharmacological treatments, e.g. parathyroid hormone (Campbell et al., 2014; Lu et al., 2017). The gold standard for evaluating how the tibia morphology and density change over time is *in vivo* micro-Computed Tomography (microCT) imaging, which allows to acquire high resolution images of the bone at different time points and to account for intrinsic variability among animals (Bouxsein et al., 2010; Dall'Ara et al., 2016). Moreover, by converting the microCT images into micro-Finite Element (microFE) models (van Rietbergen et al., 1995) the bone mechanical behavior under loading can be predicted non-invasively. Nevertheless, before their application in preclinical assessments, such models should be validated against accurate experiments. The prediction of bone stiffness by microFE models has been extensively validated for trabecular bone specimens (Schwiedrzik et al., 2016; Wolfram et al., 2010) and human vertebral bodies (Dall'Ara et al., 2012). However, quantifying the local strains over the bone volume in a spatially resolved fashion is relevant to investigate bone adaptation. It has been shown that remodeling seems mechano-regulated by the local strains, both in the mouse tibia (Birkhold et al., 2016) and in the caudal vertebra (Schulte et al., 2013). Therefore, validating the microFE predictions at the local level is fundamental in order to obtain reliable information about the local

* Corresponding author.
E-mail addresses: s.oliviero@sheffield.ac.uk (S. Oliviero), m.giorgi@sheffield.ac.uk (M. Giorgi), e.dallara@sheffield.ac.uk (E. Dall'Ara).

https://doi.org/10.1016/j.jmbbm.2018.06.022
Received 14 March 2018; Received in revised form 29 May 2018; Accepted 15 June 2018
Available online 18 June 2018

Table 1
Overview of the properties of the tested right mouse tibiae dissected from female C57BL/6J mice. For each specimen group, age, length, total bone mineral content (BMC) and tissue mineral density (TMD) are reported.

	Group	Age (weeks)	Length (mm)	BMC (mg)	TMD (mgHA/cc) Mean ± SD
Sample1	Ovariectomy	22	18.57	16.77	1078 ± 222
Sample2	Ovariectomy	22	18.70	16.66	1058 ± 216
Sample3	Wild type	24	17.95	16.74	1119 ± 228
Sample4	Wild type	24	17.09	14.26	1094 ± 221
Sample5	Wild type	16	17.76	14.51	1051 ± 225
Sample6	Wild type	16	17.63	14.23	1034 ± 219

mechanical environment engendered in the bone under loading.

Strain gauges, digital image correlation (DIC) and digital volume correlation (DVC) can be used to measure local displacements and strains of loaded bone specimens (Grassi and Isaksson, 2015). On the mouse tibia, strain gauge measurements have been performed for both determining the local strain engendered by an external load and for validating microFE predictions (Patel et al., 2014; Razi et al., 2015; Stadelmann et al., 2009; Yang et al., 2014). The main limitation of this method is that only a few strain gauges can be attached on a single tibia due to its small size (maximum of three strain gauges in (Patel et al., 2014) and in (Stadelmann et al., 2009)), and the measurement obtained represents the average strain over a relatively large area (typical size of the active gauge = 0.38 mm x 0.50 mm). Additionally, strain gauges should be ideally applied on flat surfaces, hard to find in the mouse tibia and the attachment of the sensor itself may cause a local stiffening of the specimen, as shown on the mouse forearm (Begonia et al., 2017). Digital Image Correlation (DIC) is a contactless method based on the acquisition of several images of the sample during the mechanical test, which are then used to retrieve the displacement field. The surface of the sample is conveniently speckled in order to create a random pattern, which is subsequently used to identify corresponding points in the two images based on an image correlation approach. DIC has been applied on the mouse tibia in order to quantify the distribution of strains on the surface during loading (Sztefek et al., 2010) and the sensitivity of the technique to different parameters (e.g. speckle size and density) has been analyzed (Carriero et al., 2014). DIC measurements have also been compared to microFE predictions of strains on the mouse tibia surface (Pereira et al., 2015) and on the mouse ulna and radius (Begonia et al., 2017). However, DIC can only provide measurements on a portion of the external surface of the sample. In order to overcome this limitation, Digital Volume Correlation (DVC) can be applied to two (or more) microCT images of the sample acquired during stepwise loading (Bay et al., 1999). A deformable registration approach calculates the local displacements over the whole volume of the specimen that can be differentiated into a strain field. DVC has been applied to trabecular bone samples (Chen et al., 2017; Gillard et al., 2014; Roberts et al., 2014; Zauel et al., 2005), human vertebra (Hussein et al., 2012), porcine vertebra (Costa et al., 2017), but it has never been applied on the mouse tibia. The main limitation of DVC is the need of finding a compromise between measurement accuracy and spatial resolution of the method (Dall'Ara et al., 2014, 2017). While for displacement measurements a good compromise can be found, acceptable uncertainties in strain measurements can only be obtained at very coarse resolutions (Grassi and Isaksson, 2015; Palanca et al., 2015).

The aim of this study was to use the DVC technique to validate local displacements predicted by microFE models in the mouse tibia under compression. Additionally, global stiffness and strength were estimated from microFE models and compared to the experimental measurements.

2. Materials and methods

For the validation of microFE models of the mouse tibia a similar procedure previously applied for trabecular bone (Chen et al., 2017) and porcine vertebral bodies (Costa et al., 2017) was used. Mouse tibiae were stepwise compressed within a microCT scanner, in order to acquire images of the tibiae in different loading configurations. Afterwards, a deformable registration was applied to the microCT images to compute the displacement field. MicroFE models were generated from the microCT images acquired in the preloaded configuration. Experimental and numerically predicted displacements were compared at corresponding locations. Also, global stiffness and strength predicted from microFE models were compared to the experimental measurements.

2.1. Sample preparation

Six right mouse tibiae were obtained from C57BL/6J female mice used for previous studies (Lu et al., 2015, 2017) (Table 1). Tibiae were dissected from 22-weeks-old mice which underwent ovariectomy at week 14 of age (Lu et al., 2015) (N = 2), from 24-weeks-old wild type mice (N = 2), and from 16-weeks-old wild type mice (N = 2). After carefully removing soft tissues with a scalpel, the tibiae were kept frozen at − 20 °C until testing. Total bone mineral content (BMC) and tissue mineral density (TMD) were computed from the microCT scans of the specimens as described below.

In order to align and grip the samples to the loading device, the extremities of the tibiae were embedded in resin (Technovit 4071, Kulzer, Germany) (Fig. 1A). Dissected tibiae were defrosted at room temperature in saline solution for 2 h and subsequently dehydrated in air for 1 h for the embedding. The total length was measured using a caliper. The longitudinal axis of the tibia was visually aligned to a vertical reference and the distal end was embedded in resin until the 10% of the total length. The same procedure was applied to embed the proximal end. After embedding both ends in resin, the tibia was frozen again until testing.

2.2. Stepwise compression tests and microCT imaging

Each embedded tibia was defrosted, rehydrated in saline solution for 3 h and then placed in the loading device (Fig. 1B) wrapped in a saline solution-soaked gauze, in order to avoid dehydration during the test. The loading device was placed into a microCT system (VivaCT 80, Scanco Medical, Bruettisellen, Switzerland). Stepwise compression tests were performed by means of a screw-ball joint and the axial load was measured with a 100 N load cell (C9C, HBM, United Kingdom). In order to reduce the effect of relaxation, at each load step the microCT image acquisition was started after 25 min. The procedure was repeated for four different load levels (Fig. 1C): axial load of 0.5 N to avoid moving artifacts during the scan (hereafter referred to "Preload"); axial load of 6.5 N in the elastic range, defined as half of the typical one applied during *in vivo* loading of the mouse tibia (De Souza et al., 2005) (hereafter referred to "LoadStep1" or "LS1"); axial load of 13.0 N, representative of a typical load applied in *in vivo* tibia loading experiments (De Souza et al., 2005) (hereafter referred to "LoadStep2" or "LS2"); axial load of 19.5 N to study the inelastic range (hereafter referred to "LoadStep3" or "LS3"). In total four microCT images were acquired for each sample. After the stepwise compression test, the tibia

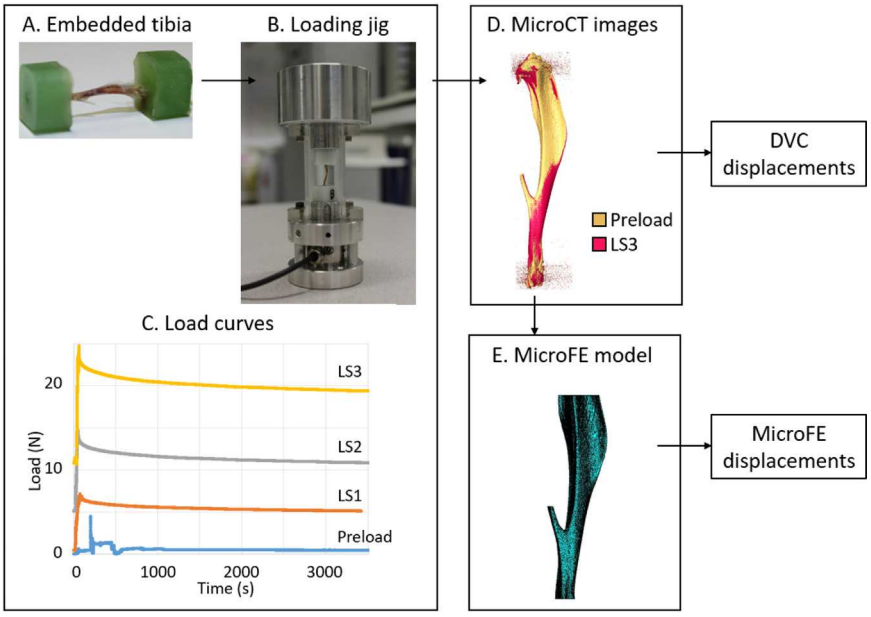

Fig. 1. Overview of the methods. Extremities of the tibiae were embedded in resin (A). After rehydration, the sample was placed into the loading device (B). Tibiae were stepwise compressed at four load levels (C): 0.5 N (preload), 6.5 N (LS1), 13.0 N (LS2) and 19.5 N (LS3). At each load level, after relaxation a microCT image was acquired and registered to the preload one (D). MicroFE models (E) were developed from the images in the preload configuration.

was loaded until failure and strength was measured as the peak load before failure. The scanning protocol (55 kVp voltage, 145 μA intensity, 10.4 μm voxel size, 100 ms integration time, 32 mm field of view, 750 projections/180°, 0.5 mm Al beam hardening filter, no frame averaging) was suitable for *in vivo* application and was previously defined as an acceptable compromise between nominal radiation dose and the accuracy in measuring the bone properties (Oliviero et al., 2017). MicroCT images were reconstructed using the software provided by the manufacturer (Scanco Medical AG) and applying a beam hardening correction based on a phantom of 1200 mg HA/cc density, which has been shown to improve the local tissue mineralization measurement (Kazakia et al., 2008).

The greyscale images of the samples in the preload configuration were converted into tissue mineral density (TMD) by using the procedure suggested by the manufacturer of the microCT scanner, based on weekly quality checks performed on a densitometric phantom with five insertions (800, 400, 200, 100 and 0 mgHA/cc equivalent density, respectively). Bone mineral content (BMC) in each voxel was obtained as its TMD multiplied by the volume of the voxel. Total BMC (Table 1) was the sum of BMC in each bony voxel of the whole tibia. Additionally, mean and standard deviation of TMD over the bony voxels are reported (Table 1).

The interested readers are welcome to contact the corresponding author who will share the data used in this study *(more details in https://figshare.com/s/3ef49956de3ef748730c)*.

2.3. Rigid registration

MicroCT images were aligned using a rigid registration procedure by using as reference the image of each sample in the preload configuration (Fig. 1D). Since during the mechanical test the embedded distal end of the tibia was fixed and the load was applied from the proximal side, in the rigid registration we aimed at maximizing the alignment of the distal portion between the loaded and preloaded images. The distal portion of the tibia until the tibio-fibular junction were rigidly registered in Amira (Amira 6.0.0, FEI Visualization Sciences Group, France) using Normalized Mutual Information as optimization criterion (Birkhold et al., 2014). The transformation matrix obtained was applied to the original greyscale image, which was subsequently resampled using Lanczos interpolator (Birkhold et al., 2014).

2.4. DVC analyses

After the rigid registration, a deformable registration toolkit (Sheffield Image Registration Toolkit, ShIRT) (Barber and Hose, 2005; Barber et al., 2007; Khodabakhshi et al., 2013) was applied to compute the displacement field over the whole volume of the tibia for each load step. Briefly, in ShIRT a grid, with distance between the nodes of each cell equal to a selectable nodal spacing (NS), is overlapped to both the preload and deformed images. The registration equation is solved at the nodes of the grid by assuming trilinear interpolation within each cell. In this study a NS of 50 voxels (520 μm) was used, for which the precision of the displacement measurements was smaller than 2.5 μm in all three directions (Appendix A). A mask was used in order to exclude the background from the analysis, which was defined from the binary images of the samples by applying dilation (imdilate function, square structuring element of 50 × 50 pixels, Matlab) and filling (imfill function, Matlab) algorithms.

The repeatability of DVC measurements of displacements was evaluated by performing three repetitions of the rigid and deformable registration procedures on one sample (Appendix B). Measurements obtained from different repetitions were highly correlated ($R^2 > 0.99$) and percentage root mean square differences (RMSD%) were in the range of 1–9% of the measured values (Appendix B).

2.5. MicroFE models

MicroFE models were created from the microCT images in the preloaded configuration (Fig., 1E). The embedded extremities of the tibia were identified from the images and excluded from the model (resulting in the exclusion of the growth plates). The cropped images were segmented using a global threshold, which was defined as the average of the grey levels corresponding to the bone and background peaks in the image frequency plot (histogram, (Chen et al., 2017, Christiansen, 2016)). Each bone voxel was converted into an 8-noded hexahedral element with isotropic linear elastic material properties. Young's Modulus of 14.8 GPa and Poisson's ratio of 0.3 were assigned (Webster et al., 2008). Boundary conditions were assigned by interpolating the DVC displacements at the proximal and distal ends of the microFE model (Chen et al., 2017), using a trilinear interpolation (CBDOF function, ANSYS Academic Research, Release 15.0). MicroFE models contained approximately 7 million elements and required about 2 h CPU time for each simulation (HPC Iceberg, INSIGNEO, University

of Sheffield; 8 cores, maximum memory = 48 Gb).

2.6. Comparison between computational predictions and experimental measurements

Displacements obtained from DVC and microFE predictions were compared over the volume of the tibia at corresponding locations, identified as the nodes of the DVC grid located inside the microFE mesh (which by construction were the centroids of the finite elements). In order to exclude the effect of boundary conditions, the comparison was performed in the middle 75% of the total length of the microFE model in the longitudinal direction.

Linear regression analysis was used to estimate the relationship between measured and computed displacements (magnitude and Cartesian components). Outliers were defined using the Cook's distance method (Fox and Long, 1990): for each specimen, load step and direction, data points having Cook's distance higher than five times the mean Cook's distance were excluded from the analysis (Chen et al., 2017; Costa et al., 2017). For each sample, load step and direction, the following parameters of the regression have been computed: slope, intercept, coefficient of determination (R^2), root mean square error (RMSE), percentage root mean square error (RMSE%, calculated as percentage of the maximum absolute experimental value), maximum error (E.max) and maximum percentage error (E.max%, calculated as percentage of the maximum absolute experimental value).

2.7. Structural mechanical properties

Apparent stiffness and strength were measured and estimated from each model. Experimental stiffness was calculated by dividing the peak force measured during the mechanical test by the average displacement in the longitudinal direction obtained from the DVC in LoadStep2. Similarly, the microFE global stiffness was estimated from LoadStep2 dividing the sum of the reaction forces along the longitudinal direction at the boundary surface by the average displacement along the longitudinal direction.

Experimental strength was measured during the mechanical test as the maximum load before failure of the tibia. From the linear microFE models, strength was estimated by assuming that the tibia fails when 2% of the nodes reach a critical strain (adapted from (Pistoia et al., 2002)) of either − 10300 με in compression or 8000 με in tension (Bayraktar et al., 2004), and rescaling the predicted reaction force accordingly.

3. Results

3.1. Local displacements

After the analysis of outliers, less than 8% of the comparison points were excluded and the final number of points was in the range of 24–53 depending on the specimen. The linear regressions between the Cartesian components (UX, UY, UZ) and magnitude (||U||) of the displacements predicted by microFE models and experimentally measured by the DVC are reported in Fig. 2 for each specimen. Statistical parameters computed for each regression analysis are reported in Table 2. The magnitudes of predicted displacements were highly correlated with the corresponding experimental measurements ($R^2 > 0.82$ in all cases). Slopes of the regression lines were in the range of 0.69–0.95, indicating that microFE models tended to overestimate local predictions for increasing absolute displacements. Root mean square error varied according to the sample from 5% to 22% and no apparent effect of load level was observed. Higher variability and generally lower correlations were found for the Cartesian components. Displacements in the longitudinal direction Z showed fair to optimal correlations with the experimental ones, with R^2 in the range of 0.69–0.92 (with the exception of Sample1 in LoadStep1, for which $R^2 = 0.53$ was found, as discussed later). Slopes of the regression lines were in the range of 0.50–0.97 (with the exception of Sample1 in LoadStep1, for which slope = 0.26, as discussed later), indicating an overestimation of local displacements in the loading direction, similarly to what observed for the displacement magnitude. Slopes for the transverse directions were in the range of 0.76–1.70 and 0.80–1.42 respectively, and errors were higher (RMSE of 6–60% for displacements along X and 10–81% along Y) compared to those computed along the longitudinal direction (RMSE of 6–41%). Absolute errors tended to increase with the load level: for LoadStep1 RMSE in the longitudinal direction was lower than 7 μm for all samples, while for LoadStep3 RMSE up to 23 μm was observed. However, percentage errors were comparable for all load steps.

The spatial distribution of the longitudinal displacement values over the tibia is reported in Fig. 3 for Sample1 (best slope, equal to 0.96) and Sample4 (worst slope, equal to 0.53) in LoadStep3. For Sample1, displacements were more homogeneously distributed over the tibia and the microFE model provided good predictions (slope = 0.96, $R^2 = 0.80$). For Sample4, the distribution of displacements was more heterogeneous over the tibia, with higher gradients at the proximal side compared to the distal side, and microFE models tended to overestimate the local displacements (slope = 0.53), even though correlation was good ($R^2 = 0.77$). The mode of deformation tended to differ between DVC measurements and microFE predictions, showing more accentuated bending in the second case, in the sagittal plane. Therefore, the comparison points characterized by the highest errors were located either in the anterior region of the tibia (corresponding to the tibial ridge) or in the posterior one (Fig. 3).

3.2. Structural mechanical properties

Apparent mechanical properties experimentally measured and predicted by microFE models are reported in Fig. 4. Every sample was predicted to fail in compression. The absolute errors were 14% ± 11% for stiffness predictions and 9% ± 9% for strength predictions.

3.3. Strain distribution

Histograms (frequency plots) and spatial distributions of strains obtained from microFE models for each load step are reported in Fig. 5 and Fig. 6 (for Sample2 and Sample3, for which the lowest and highest local strains were found respectively).

Absolute strains were higher in compression compared to tension in all load steps (Fig. 5). The spatial distribution of strains over the tibia was similar for all samples, with peaks of compressive strains located at the distal extremity on the antero-medial surface and around the mid-diaphysis at the postero-lateral apex (Fig. 6). However, strain values varied among the samples. In LoadStep2 (representative of the typical load applied during *in vivo* loading of the mouse tibia (De Souza et al., 2005)), the peak corresponding to the high strains in the histograms (Fig. 5) varied from − 2330 με to − 4825 με among samples. In LoadStep3, some nodes exhibited strain values above the considered yield strain (−10300 με in compression (Bayraktar et al., 2004)). In Sample1, 4, 5 and 6 the portion of nodes overcoming the yield strain was less than 1%, while for Sample3 (Fig. 5) it was 2.6% of the total. No strains above the yield value were observed in Sample2 (Fig. 5).

4. Discussion

The goal of this study was to compare the local and structural mechanical properties predicted by microFE models in the mouse tibia under compression with experimental datasets, obtained using a combination of *in situ* mechanical testing, microCT imaging and the Digital Volume Correlation (DVC).

Apparent mechanical properties of the tibia estimated from microFE models were in good agreement with experimental measurements for stiffness (differences of 14% ± 11%) and strength (9% ± 9%),

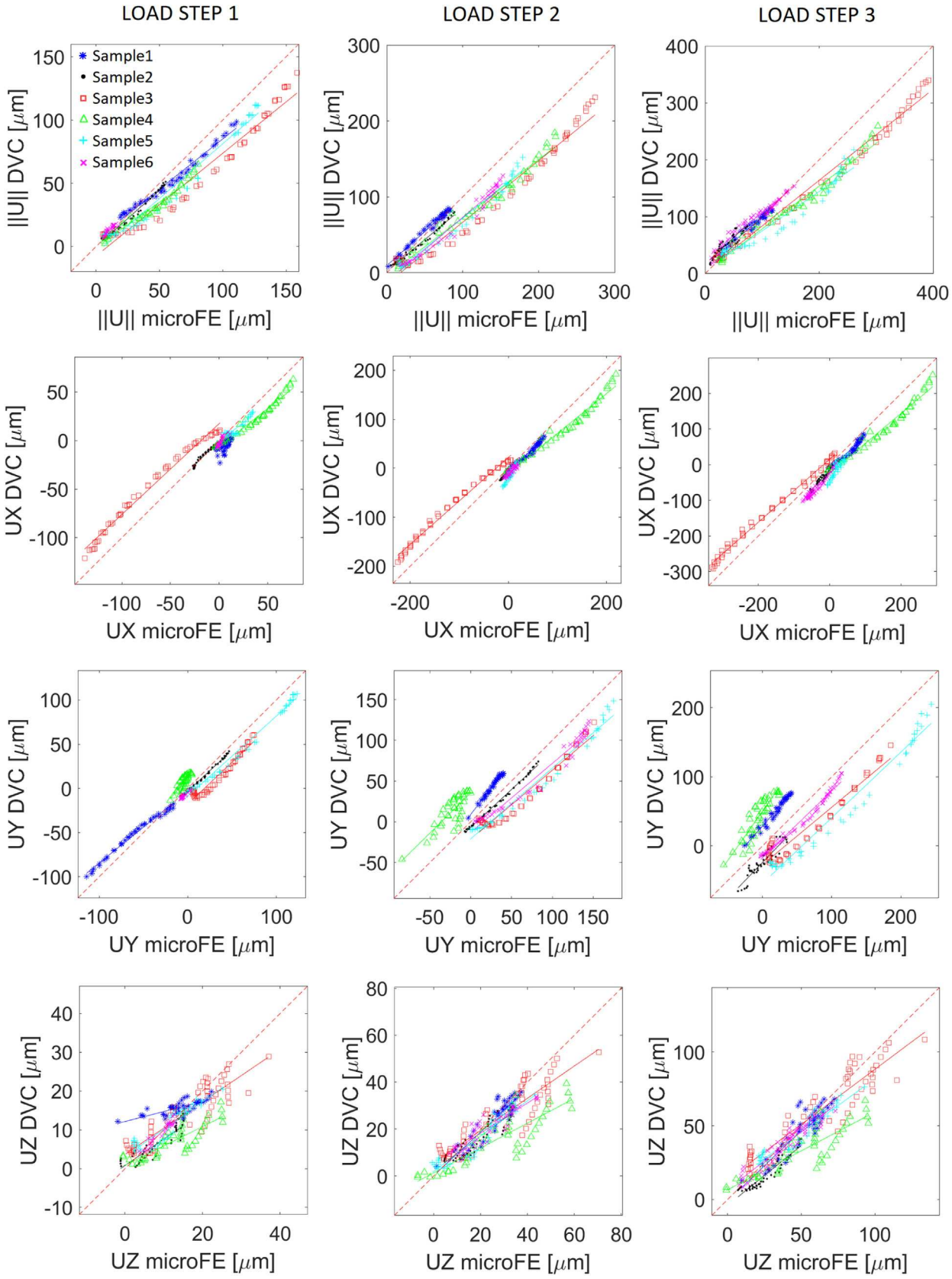

Fig. 2. Magnitude and Cartesian components of the displacements measured from the DVC analysis and predicted by the microFE models. Regression lines are reported for each sample (different colours as reported in the legend). The 1:1 relationship is plotted in red dashed line.

Table 2
Parameters of the regression analysis for each sample and each load step along the three directions and in magnitude. For each regression slope, intercept (Int), coefficient of determination (R^2), root mean square error (RMSE), percentage RMSE, maximum error (E.max) and percentage E.max are reported.

	Load Step 1				Load Step 2				Load Step 3			
	X	Y	Z	||U||	X	Y	Z	||U||	X	Y	Z	||U||
Sample1												
Slope	0.76	0.81	0.26	0.79	0.89	1.30	0.92	0.90	0.91	1.14	0.96	0.86
Int[μm]	− 10	− 3	12	6	− 5	9	0	9	− 11	29	− 1	13
R^2	0.37	0.99	0.53	0.98	0.97	0.98	0.84	0.99	0.95	0.97	0.80	0.97
RMSE[μm]	12	10	4	9	11	17	4	5	18	32	8	6
RMSE[%]	52	10	22	9	16	29	11	6	21	42	11	5
E.max[μm]	24	15	14	14	20	23	8	9	34	38	17	13
E.max[%]	103	15	70	14	31	39	22	10	40	49	24	11
Sample2												
Slope	1.00	0.93	0.68	0.89	1.14	0.93	0.73	0.84	1.13	1.04	0.81	0.95
Int[μm]	0	− 3	1	0	− 6	− 7	2	2	− 14	− 24	− 4	16
R^2	0.96	1.00	0.81	0.99	0.98	1.00	0.83	0.99	0.89	0.85	0.86	0.85
RMSE[μm]	2	5	3	4	7	10	5	7	18	25	10	16
RMSE[%]	6	11	21	8	27	13	15	9	23	38	24	19
E.max[μm]	4	7	7	8	9	14	12	12	28	38	17	27
E.max[%]	13	17	49	15	38	18	37	15	36	57	40	32
Sample3												
Slope	0.93	0.95	0.68	0.81	0.89	0.85	0.69	0.81	0.88	0.83	0.75	0.80
Int[μm]	17	− 18	4	− 7	22	− 21	6	− 15	16	− 27	14	4
R^2	0.99	0.94	0.80	0.96	0.99	0.94	0.80	0.97	0.99	0.93	0.86	0.99
RMSE[μm]	23	20	5	26	36	34	9	46	38	42	14	46
RMSE[%]	19	34	16	19	19	28	17	20	13	29	13	13
E.max[μm]	30	27	12	36	52	45	20	64	64	57	34	75
E.max[%]	25	45	43	27	27	37	39	27	22	39	31	22
Sample4												
Slope	0.80	1.23	0.50	0.71	0.81	0.99	0.53	0.77	0.84	1.42	0.53	0.75
Int[μm]	− 7	12	1	0	− 10	35	1	− 4	− 24	50	7	3
R^2	0.96	0.68	0.69	0.96	0.97	0.67	0.75	0.97	0.97	0.80	0.77	0.97
RMSE[μm]	16	12	7	14	36	37	15	36	51	50	23	44
RMSE[%]	25	70	41	22	19	81	39	20	20	63	34	17
E.max[μm]	21	18	13	22	51	50	30	55	70	68	44	67
E.max[%]	32	102	78	33	27	109	77	30	28	85	65	26
Sample5												
Slope	0.77	0.90	0.70	0.87	1.70	0.87	0.75	0.80	1.48	0.95	0.72	0.69
Int[μm]	− 1	− 9	3	− 5	− 19	− 21	2	− 8	− 40	− 54	10	6
R^2	0.86	0.99	0.83	0.97	0.90	0.98	0.89	0.97	0.79	0.97	0.92	0.94
RMSE[μm]	6	16	3	17	17	34	5	29	35	62	8	45
RMSE[%]	20	15	13	15	45	23	15	19	60	30	10	21
E.max[μm]	12	25	5	27	27	50	9	49	51	86	17	78
E.max[%]	40	24	26	24	70	34	27	32	89	42	22	36
Sample6												
Slope	1.32	0.80	0.97	0.93	0.92	0.85	0.64	0.85	1.07	0.97	0.79	0.81
Int[μm]	− 3	− 5	0	3	− 11	− 13	5	− 12	− 25	− 17	7	26
R^2	0.78	0.83	0.91	0.82	0.80	0.96	0.83	0.97	0.94	0.98	0.91	0.95
RMSE[μm]	4	4	1	3	12	28	6	27	29	20	6	14
RMSE[%]	50	32	6	16	60	23	17	21	28	19	10	9
E.max[μm]	6	5	2	5	18	48	11	44	38	29	14	32
E.max[%]	79	43	14	31	89	39	34	34	37	28	23	21

indicating that the failure criterion chosen in this study was adequate. This good agreement between experimental and predicted properties is fundamental for the credibility of the models that are used for estimating the effect of diseases and interventions *in vivo* (Lu et al., 2017).

The microFE predictions of displacements were found to be highly correlated with the experimental measurements in magnitude ($R^2 > 0.82$), while higher variability and errors were found in the Cartesian components. Correlations between the predicted and measured displacements in the longitudinal direction were fair to optimal (R^2 = 0.69–0.92). Nevertheless, the microFE models tended to overestimate local displacements in the loading direction, especially for larger absolute displacements. Similarly to previous studies (Chen et al., 2017; Costa et al., 2017; Zauel et al., 2005), errors were smaller in the loading direction compared to the transverse ones. No apparent effect of load levels was observed, with correlation parameters, slopes and percentage errors similar for all of them. By analyzing the spatial distribution of longitudinal displacements and errors, we observed that the microFE models predicted a more accentuated bending in the antero-posterior direction compared to the DVC measurements. The discrepancy in the mechanism of deformation was larger when displacements were not homogeneously distributed over the tibia (Fig. 3) and was probably the cause of the systematic errors found in the transverse direction Y (Fig. 2). This difference could potentially be due to residual errors in the registration of the microCT images, which may be affected by the geometry and features of the specimens. Since the mouse tibia is a slender bone and is characterized by a natural curvature, even a small mismatch between the experimental and microFE conditions could have an impact on the local predictions. The simplified model we have used in this study could also play a role. In particular, the assumptions about the material properties (homogeneous, isotropic and linear) may affect the predictions of the local displacements under loading and the structural mechanical properties. The same microFE modelling approach has been previously validated for trabecular bone samples (Chen et al., 2017) and porcine vertebrae (Costa et al., 2017), showing that microFE models could predict more than 87% of the variation of the local displacements in both the longitudinal and transverse

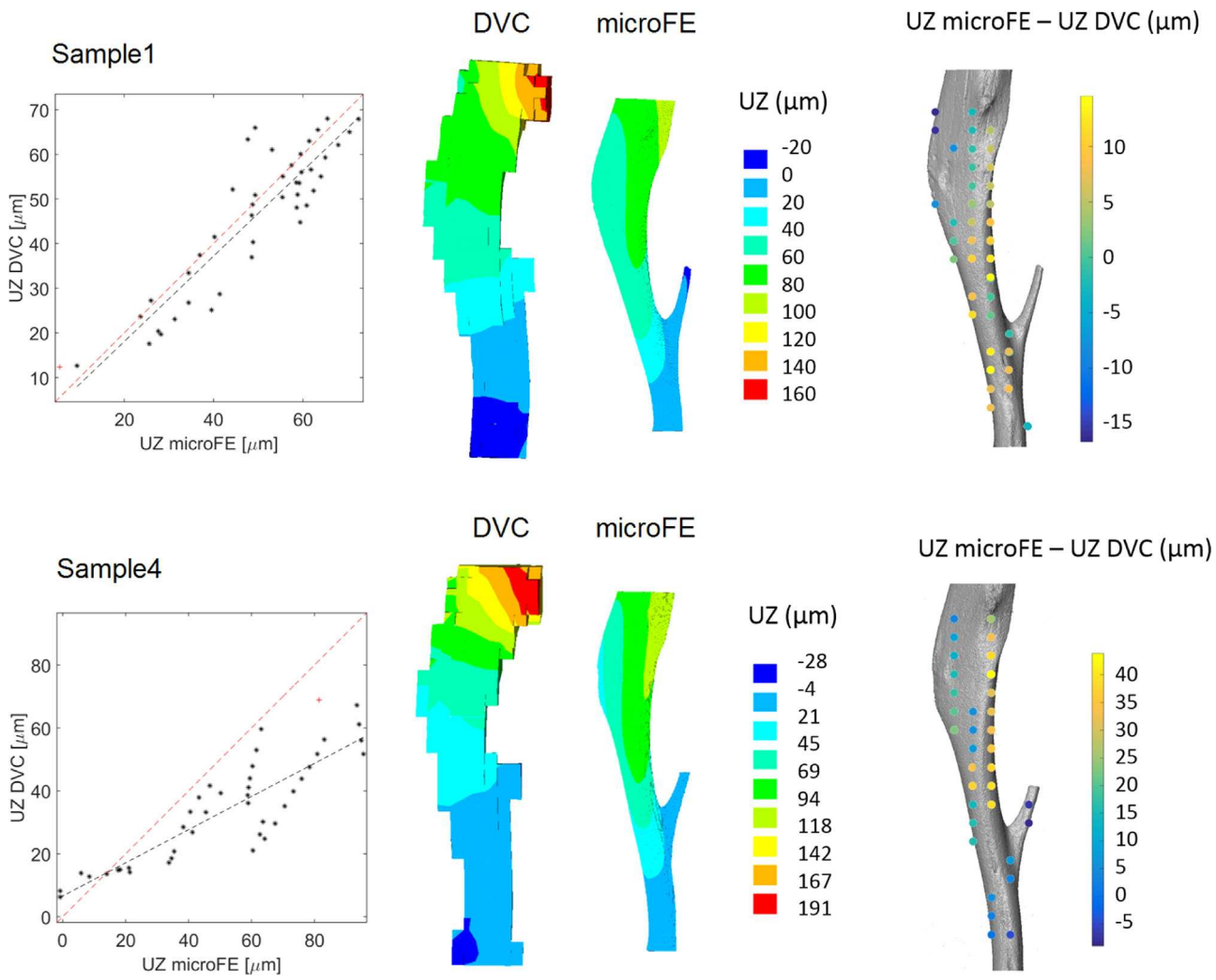

Fig. 3. Spatial distribution of the displacements along the axial direction (UZ) and corresponding errors (UZ microFE – UZ DVC) for Sample1 and Sample4 in LoadStep3. The 1:1 relationship is plotted in red dashed line, while the regression line is plotted in black.

directions. The higher errors found for the mouse tibia are probably due to the different geometry and structure of the bone: the mouse tibia is mainly made of cortical bone, therefore the local material properties could be more relevant, compared to the previous cases (trabecular bone and porcine vertebrae), where the geometry and orientation of the trabeculae would probably play a major role. In particular, the higher errors found in the transverse directions compared to the longitudinal one suggest that local predictions could be improved by implementing anisotropic material properties in the models.

For Sample1 very low slope of the regression line and low correlation (slope = 0.26, R^2 = 0.53) were found in LoadStep1, due to large differences between measured and predicted displacements in a

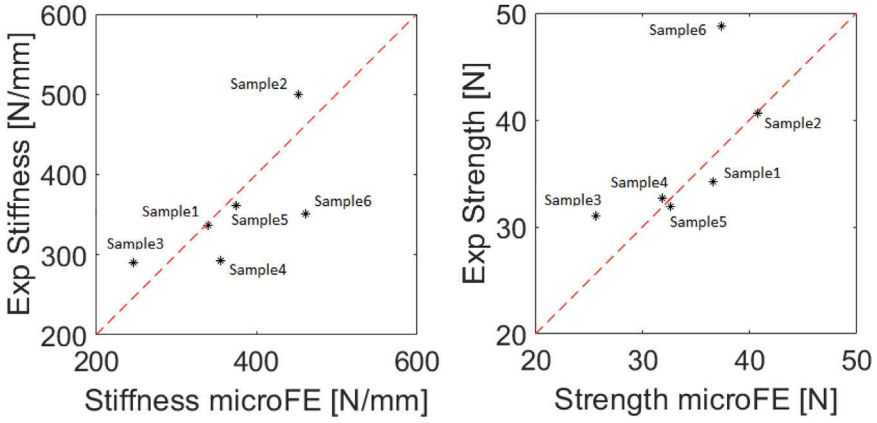

Fig. 4. Comparison between stiffness (left) and strength (right) measured experimentally and predicted by the microFE models in LoadStep2. The 1:1 relationship is plotted in red dashed line.

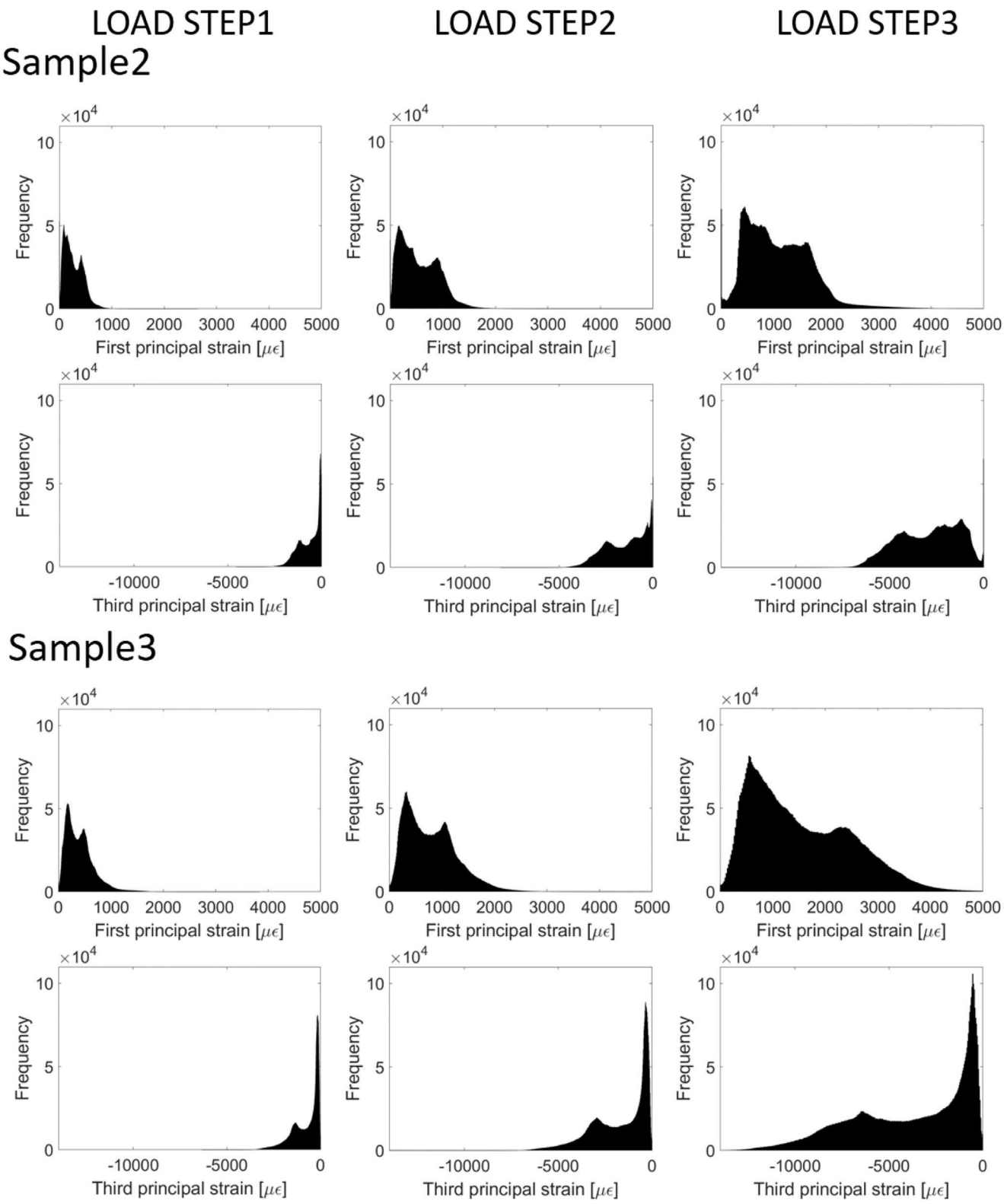

Fig. 5. Histograms of first and third principal strains obtained from microFE models of Sample2 and Sample3, which exhibited the lowest and highest local strains respectively.

subgroup of the investigated points (Fig. 7). The high errors were located at the anterior tibial ridge (Fig. 7), which may be related to the lower local accuracy of the DVC measurement (Appendix C). Additionally, the smaller deformations the tibia undergoes in LoadStep1 could potentially be harder to detect with the DVC algorithm. In fact, in LoadStep3 errors at the same comparison points were lower (24% in LS3 compared to 70% in LS1). Overall, considering the good agreement between the predictions of the models and the experimental measurements of displacements, the application of this approach to estimate local strains to predict bone remodeling (Birkhold et al., 2016; Schulte et al., 2013) seems adequate.

Strain distributions obtained with microFE models showed high

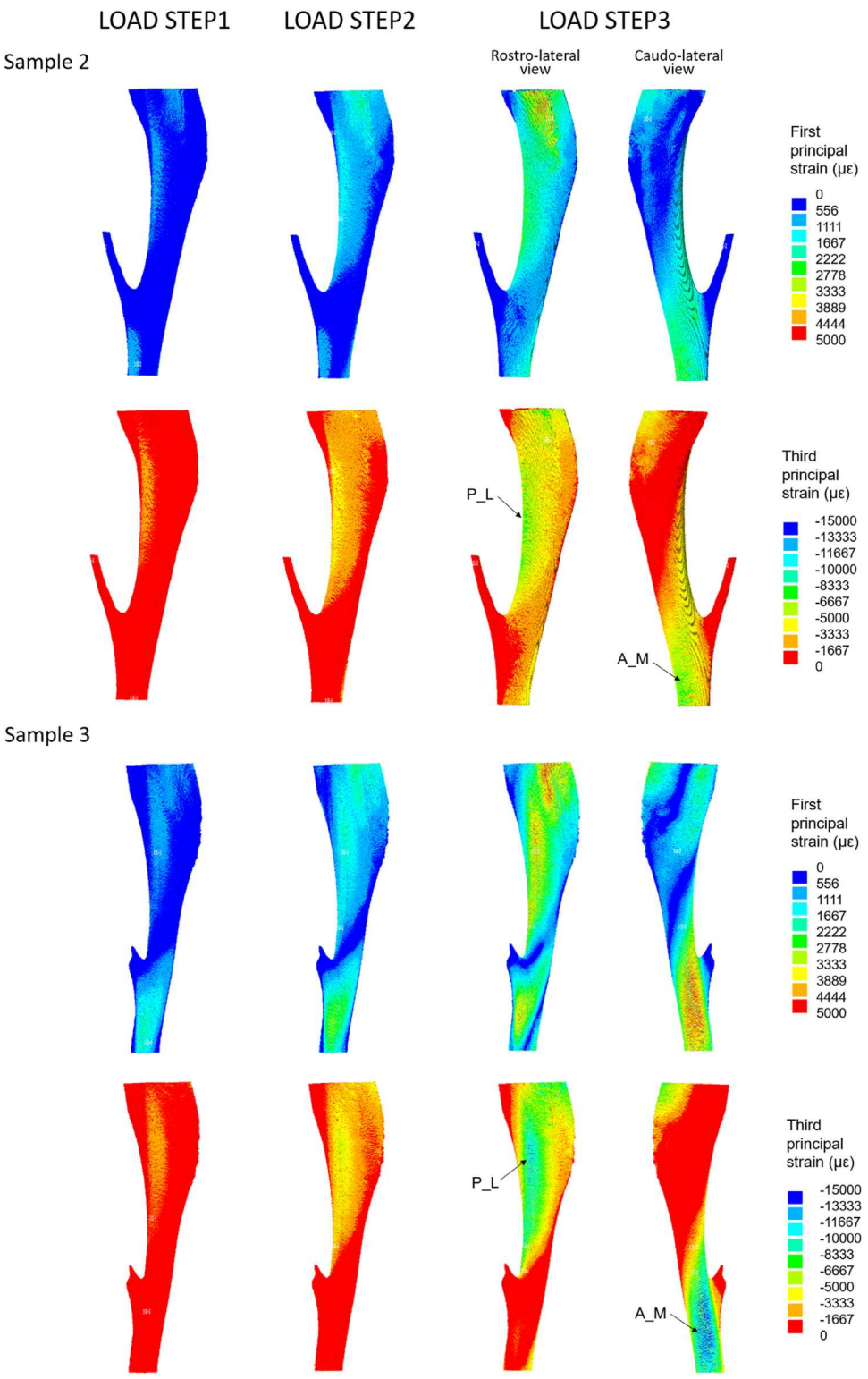

Fig. 6. Spatial distribution of first and third principal strains for Sample2 and Sample3, for which the lowest and highest local strains were observed respectively. Peaks of compressive strains were located at the distal extremity on the antero-medial (A_M) surface and around the midshaft at the postero-lateral (P_L) apex.

variability among samples, with peak strains ranging from − 2330με to − 4825με in LoadStep2, although the same nominal loading conditions were applied. Additionally, the peak compressive strains were not consistently located in the same region for all tibiae, but were either around the mid-diaphysis at the postero-lateral apex or at the distal extremity on the antero-medial surface (Fig. 6). The load applied during *in vivo* loading of the mouse tibia is normally selected by targeting a peak tensile strain of 1200–1500 με at the midshaft on antero-medial surface, which results in peak strains of − 2300με to − 3000με in compression (Birkhold et al., 2016; Patel et al., 2014). For studies performed on mice of the same strain (age range of 10–78 weeks) axial loads applied to the tibia to induce such local strain levels were 9–13 N in compression (Birkhold et al., 2016; De Souza et al., 2005; Patel et al., 2014). Even if similar axial loads were used in these studies, it should

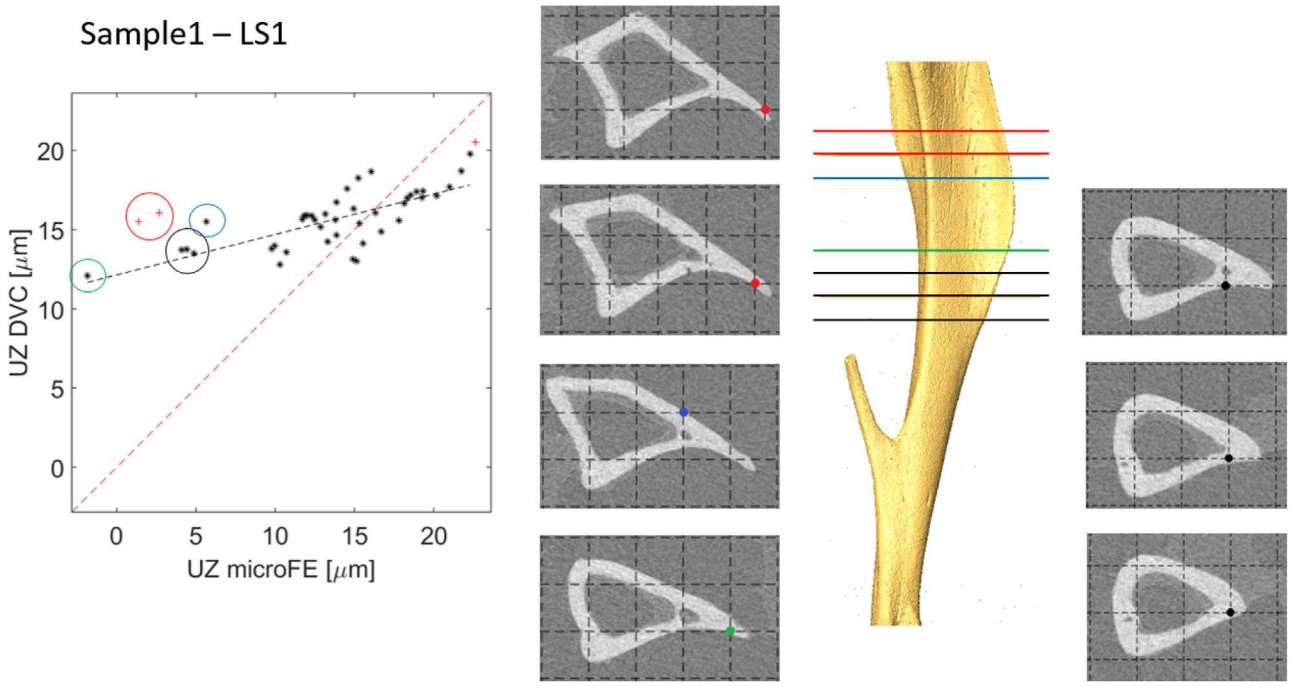

Fig. 7. Spatial location of the comparison points characterized by highest errors in the longitudinal displacement prediction (Sample1, LoadStep1). Outliers are reported as red crosses.

be noticed that the loading condition applied to the tibia is different in the two cases: axial load on the dissected tibia versus more complex loading scenario for *in vivo* loading, where fibula and soft tissues are intact. Also, a dehydration and rehydration procedure was performed on the tibiae in this study, in order to embed the extremities in resin and align the sample to the loading device. This could affect the material properties on the bone. Therefore, the strain distributions obtained in this study may be different from those experienced by the bone *in vivo*. Nevertheless, our results highlight the importance of taking into account the realistic loading conditions applied on the tibia during loading, which would probably differ from the nominal ones.

The main limitation of this work is that the complex validation method limited its applicability to a small sample size (N = 6). Also, bones from mice of different ages and interventions were included in order to test the model in different conditions, which may have increased the variability of the results. Nevertheless, it should be noticed that all samples were from mice considered skeletally mature (age of 16–24 weeks), therefore we do not expect this to have a major impact on the validation study. Another limitation is that in this study simple (but efficient) homogeneous isotropic linear voxel based microFE models were used. Further improvements of the models are currently under exploration: implementing heterogeneous material properties based on local mineralization could improve the predictions of structural properties and anisotropic material properties could improve local predictions in the transverse directions. Also, we are planning to improve the boundary recovery by using tetrahedral meshes and add material non-linearities for improving the failure criterion. Nevertheless, while these improvements may lead to a reduction of the peak errors found in some of the regions of the bone, the application of the simple microFE models tested in this study showed errors acceptable for most applications. Lastly, the validation of the microFE predictions was limited to displacements and not strains, due to the current limitations of microCT-based DVC measurements. In a recent work (Palanca et al., 2017) it has been shown that the precision of DVC strain measurements becomes acceptable for a spatial resolution of 120 μm (within the mouse cortical bone) if the method is based on Synchrotron Radiation microCT images. However, the combination of DVC and Synchrotron Radiation tomograms is intrinsically limited, since the high radiation would potentially damage the organic phase of the bone.

In conclusion, we have developed and applied a procedure to validate microFE predictions of local internal displacements and apparent mechanical properties of the mouse tibia under compression, based on digital volume correlation (DVC). An overall good agreement was found between the numerical predictions and experimental measurements, highlighting the potential of the method to provide non-invasive estimation of mechanical properties for preclinical analyses of bone properties.

Acknowledgements

The study was funded by the Engineering and Physical Sciences Research Council (EPSRC, MultiSim project, Grant number: EP/K03877X/1) and the National Centre for Replacement, Refinement and Reduction of Animals in Research (NC3Rs, Grant numbers: NC/K000780/1 and NC/R001073/1). The authors gratefully acknowledge Simon Rawson and John Wilson for manufacturing the jig, Dr Gareth Fletcher for implementing the DVC service, and the skelet. AL laboratory for access to the scanning facilities.

Declaration statementsConflict of interest

None declared.

Appendix A

The aim of this analysis was to evaluate the uncertainties of the DVC measurement of displacements and strains, in order to define a suitable nodal spacing (NS) for the validation study on the mouse tibia. Two pairs of repeated scans were used. Sample2 was scanned twice in the preload

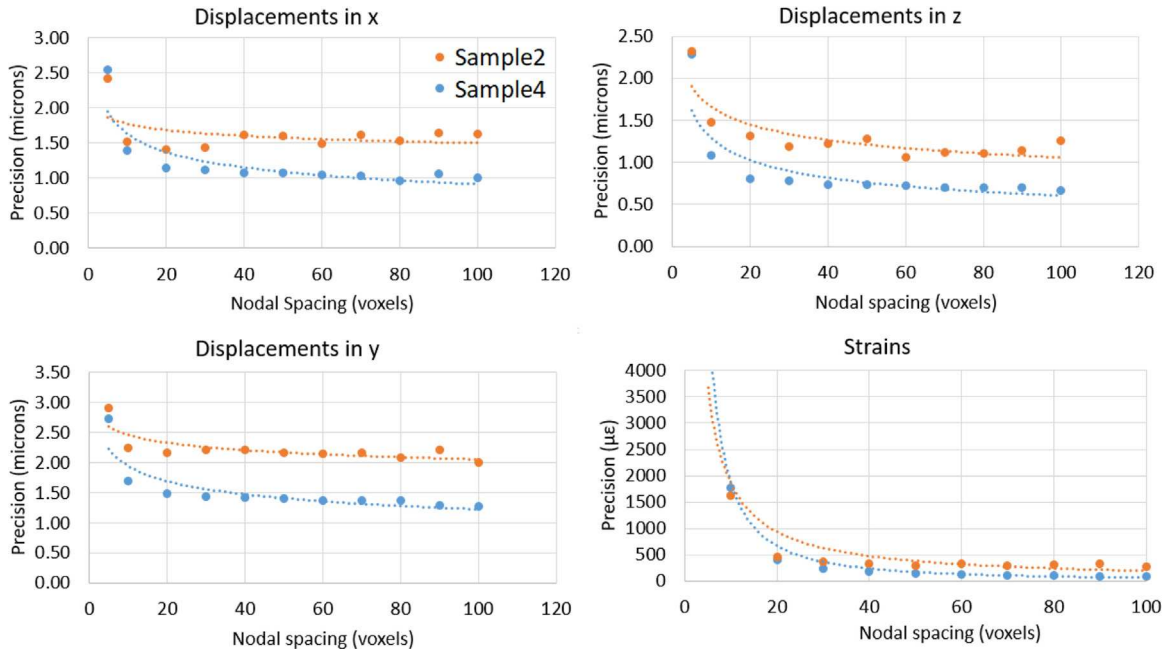

Fig. A.1. Precision error of DVC displacements and strains in function of nodal spacing, obtained using repeated scans on Sample2 (orange) and Sample4 (blue).

Table B.1
Parameters of the regression analysis comparing DVC measurements of local displacements obtained from three different repetitions of the image processing procedure. For each regression slope, intercept, coefficient of determination (R^2), root mean square difference (RMSD), percentage RMSD, maximum difference (D.max) and percentage D.max are reported.

Repetition 1 vs repetition 2			
	X	Y	Z
Slope	0.99	1.10	0.97
Intercept [μm]	2	7	2
R^2	1.000	0.999	0.999
RMSD [μm]	2	12	2
RMSD %	1	8	3
D.max [μm]	3	19	2
D.max %	2	13	4
Repetition 1 vs repetition 3			
	X	Y	Z
Slope	1.05	0.98	1.04
Intercept [μm]	− 4	2	0
R^2	0.999	0.999	0.997
RMSD [μm]	9	2	1
RMSD %	5	2	3
D.max [μm]	20	5	4
D.max %	10	4	7
Repetition 2 vs repetition 3			
	X	Y	Z
Slope	1.06	0.89	1.07
Intercept [μm]	− 6	− 5	− 2
R^2	0.999	0.997	0.996
RMSD [μm]	11	11	1
RMSD %	6	9	2
D.max [μm]	22	17	3
D.max %	11	14	5

configuration. Sample4 was scanned twice in a loaded configuration (LoadStep2, 13.0 N axial load). Repeated images were rigidly registered and the DVC algorithm was applied using 11 different NS values ranging from 5 to 100 voxels. Precision error was calculated as the standard deviation of the displacements in each direction (Palanca et al., 2015). Precision of strains measurement was calculated as the standard deviation of the average of the absolute values of the six strain components (Palanca et al., 2015). The analysis was performed in the middle 80% of the total length in order to reduce the boundary effects.

In Fig. A.1, precision error is reported for the displacements in the three directions and for strains in function of NS.

For NS = 50 voxels, precision errors of displacements in the three directions were lower than 2.5 μm, corresponding to one third of voxel size approximately. Additionally, the precision error of strains was smaller than 300με, which is one order of magnitude lower compared to the typical

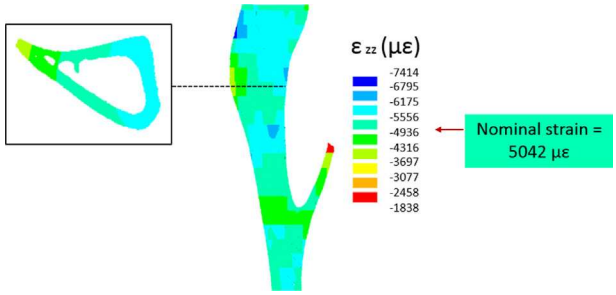

Fig. C.1. Spatial distribution of strains in the longitudinal direction (ε_{zz}) obtained by applying a virtual deformation on repeated scans of Sample2.

peak strains engendered in the mouse tibia under *in vivo* compressive loading (in the range of −2300 to −3000 με (Patel et al., 2014)).

Appendix B

The aim of this analysis was to evaluate the repeatability of DVC measurements of local displacements from microCT images. We evaluated how the image processing steps influence the measured displacements. In particular, uncertainties are due to the initial alignment of the two microCT images (preload and deformed configurations), to the rigid registration procedure and to the deformable registration. An experienced operator performed three repetitions of the image processing procedure (Sections 2.3–2.4) for one sample (Sample3, LoadStep2).

DVC measurements of local displacements obtained from different repetitions were highly correlated ($R^2 > 0.99$, Table B.1). Root mean square differences (RMSD) were in the range of 1–12 μm (1–9% of the measured value), while maximum differences (D.max) were in the range of 2–22 μm (2–14% of the measured value) (Table B.1).

Appendix C

The standard method to assess the reliability of DVC measurements is based on quantifying the uncertainties in displacements and strains calculated in a zero-strain test, in which repeated scans are performed with no deformation of the sample (see Appendix A). From this test, accuracy and precision error are evaluated over the whole region of analysis (Liu and Morgan, 2007). However, there could be areas of the sample characterized by larger local errors. The aim of this analysis was to evaluate the accuracy of local strains obtained from DVC, which is linked to the accuracy of local displacements. Repeated scans of Sample2 in the preload configuration were used. The second scan of the tibia was virtually deformed by applying a scaling factor of 0.995 in the longitudinal direction, which caused a global displacement of 94 μm (similarly to what observed for LoadStep3). In this condition, the nominal strain is known, equal to 5042 με homogeneously distributed over the tibia. The obtained image was rigidly registered to the first scan and the DVC algorithm was applied using a nodal spacing of 50 voxels. A finite element (FE) package (ANSYS Academic Research, Release 15.0) was used to calculate strains from the DVC displacements.

In Fig. C.1, the spatial distribution of strains over the tibia is reported. Strains were not homogeneously distributed over the tibia, indicating that the accuracy of the DVC method may vary depending on the spatial location, even if the global accuracy and precision are low. Peaks of error were located at the tibial ridge.

References

Barber, D.C., Hose, D.R., 2005. Automatic segmentation of medical images using image registration: diagnostic and simulation applications. J. Med. Eng. Technol. 29, 53–63.
Barber, D.C., Oubel, E., Frangi, A.F., Hose, D.R., 2007. Efficient computational fluid dynamics mesh generation by image registration. Med. Image Anal. 11, 648–662.
Bay, B.K., Smith, T.S., Fyhrie, D.P., Saad, M., 1999. Digital volume correlation: three-dimensional strain mapping using X-ray tomography. Exp. Mech. 39, 217–226.
Bayraktar, H.H., Morgan, E.F., Niebur, G.L., Morris, G.E., Wong, E.K., Keaveny, T.M., 2004. Comparison of the elastic and yield properties of human femoral trabecular and cortical bone tissue. J. Biomech. 37, 27–35.
Begonia, M., Dallas, M., Johnson, M.L., Thiagarajan, G., 2017. Comparison of strain measurement in the mouse forearm using subject-specific finite element models, strain gaging, and digital image correlation. Biomech. Model. Mechanobiol. 16, 1243–1253.
Birkhold, A.I., Razi, H., Duda, G.N., Weinkamer, R., Checa, S., Willie, B.M., 2014. Mineralizing surface is the main target of mechanical stimulation independent of age: 3D dynamic in vivo morphometry. Bone 66, 15–25.
Birkhold, A.I., Razi, H., Duda, G.N., Weinkamer, R., Checa, S., Willie, B.M., 2016. The periosteal bone surface is less mechano-responsive than the endocortical. Sci. Rep. 6, 23480.
Birkhold, A.I., Razi, H., Weinkamer, R., Duda, G.N., Checa, S., Willie, B.M., 2015. Monitoring in vivo (re)modeling: a computational approach using 4D microCT data to quantify bone surface movements. Bone 75, 210–221.
Bouxsein, M.L., Boyd, S.K., Christiansen, B.A., Guldberg, R.E., Jepsen, K.J., Müller, R., 2010. Guidelines for assessment of bone microstructure in rodents using micro–computed tomography. J. Bone Miner. Res. 25, 1468–1486.
Buie, H.R., Moore, C.P., Boyd, S.K., 2008. Postpubertal architectural developmental patterns differ between the L3 vertebra and proximal tibia in three inbred strains of mice. J. Bone Miner. Res. 23, 2048–2059.
Campbell, G., Tiwari, S., Grundmann, F., Purcz, N., Schem, C., Glüer, C.-C., 2014. Three-dimensional image registration improves the long-term precision of in vivo micro-computed tomographic measurements in anabolic and catabolic mouse models. Calcif. Tissue Int. 94, 282–292.
Carriero, A., Abela, L., Pitsillides, A.A., Shefelbine, S.J., 2014. Ex vivo determination of bone tissue strains for an in vivo mouse tibial loading model. J. Biomech. 47, 2490–2497.
Chen, Y., Dall'Ara, E., Sales, E., Manda, K., Wallace, R., Pankaj, P., Viceconti, M., 2017. Micro-CT based finite element models of cancellous bone predict accurately displacement once the boundary condition is well replicated: a validation study. J. Mech. Behav. Biomed. Mater. 65, 644–651.
Christiansen, B.A., 2016. Effect of micro-computed tomography voxel size and segmentation method on trabecular bone microstructure measures in mice. Bone Rep. 5, 136–140.
Costa, M.C., Tozzi, G., Cristofolini, L., Danesi, V., Viceconti, M., Dall'Ara, E., 2017. Micro Finite Element models of the vertebral body: validation of local displacement predictions. PLoS One 12, e0180151.
Dall'Ara, E., Barber, D., Viceconti, M., 2014. About the inevitable compromise between spatial resolution and accuracy of strain measurement for bone tissue: a 3D zero-strain study. J. Biomech. 47, 2956–2963.
Dall'Ara, E., Boudiffa, M., Taylor, C., Schug, D., Fiegle, E., Kennerley, A.J., Damianou, C., Tozer, G.M., Kiessling, F., Müller, R., 2016. Longitudinal imaging of the ageing mouse. Mech. Ageing Dev. 160, 93–116.
Dall'Ara, E., Pahr, D., Varga, P., Kainberger, F., Zysset, P., 2012. QCT-based finite element models predict human vertebral strength in vitro significantly better than simulated DEXA. Osteoporos. Int. 23, 563–572.
Dall'Ara, E., Peña-Fernández, M., Palanca, M., Giorgi, M., Cristofolini, L., Tozzi, G., 2017. Precision of digital volume correlation approaches for strain analysis in bone imaged with micro-computed tomography at different dimensional levels. Front. Mater. 4, 31.
De Souza, R.L., Matsuura, M., Eckstein, F., Rawlinson, S.C.F., Lanyon, L.E., Pitsillides, A.A., 2005. Non-invasive axial loading of mouse tibiae increases cortical bone formation and modifies trabecular organization: a new model to study cortical and

cancellous compartments in a single loaded element. Bone 37, 810–818.
Fox, J., Long, J.S., 1990. In: Fox, John, Long, J. Scott (Eds.), Modern Methods of Data Analysis. Sage Publications, Newbury Park, CA.
Gillard, F., Boardman, R., Mavrogordato, M., Hollis, D., Sinclair, I., Pierron, F., Browne, M., 2014. The application of digital volume correlation (DVC) to study the microstructural behaviour of trabecular bone during compression. J. Mech. Behav. Biomed. Mater. 29, 480–499.
Grassi, L., Isaksson, H., 2015. Extracting accurate strain measurements in bone mechanics: a critical review of current methods. J. Mech. Behav. Biomed. Mater. 50, 43–54.
Holguin, N., Brodt, M.D., Sanchez, M.E., Silva, M.J., 2014. Aging diminishes lamellar and woven bone formation induced by tibial compression in adult C57BL/6. Bone 65, 83–91.
Hussein, A.I., Barbone, P.E., Morgan, E.F., 2012. Digital volume correlation for study of the mechanics of whole bones. Procedia IUTAM 4, 116–125.
Kazakia, G.J., Burghardt, A.J., Cheung, S., Majumdar, S., 2008. Assessment of bone tissue mineralization by conventional x-ray microcomputed tomography: comparison with synchrotron radiation microcomputed tomography and ash measurements. Med. Phys. 35, 3170–3179.
Khodabakhshi, G., Walker, D., Scutt, A., Way, L., Cowie, R.M., Hose, D.R., 2013. Measuring three-dimensional strain distribution in tendon. J. Microsc. 249, 195–205.
Klinck, R.J., Campbell, G.M., Boyd, S.K., 2008. Radiation effects on bone architecture in mice and rats resulting from in vivo micro-computed tomography scanning. Med. Eng. Phys. 30, 888–895.
Liu, L., Morgan, E.F., 2007. Accuracy and precision of digital volume correlation in quantifying displacements and strains in trabecular bone. J. Biomech. 40, 3516–3520.
Lu, Y., Boudiffa, M., Dall'Ara, E., Bellantuono, I., Viceconti, M., 2015. Evaluation of in-vivo measurement errors associated with micro-computed tomography scans by means of the bone surface distance approach. MED ENG PHYS 37, 1091–1097.
Lu, Y., Boudiffa, M., Dall'Ara, E., Liu, Y., Bellantuono, I., Viceconti, M., 2017. Longitudinal effects of parathyroid hormone treatment on morphological, densitometric and mechanical properties of mouse tibia. J. Mech. Behav. Biomed. Mater. 75, 244–251.
Main, R.P., Lynch, M.E., Van Der Meulen, M.C.H., 2010. In vivo tibial stiffness is maintained by whole bone morphology and cross-sectional geometry in growing female mice. J. Biomech. 43, 2689–2694.
Oliviero, S., Lu, Y., Viceconti, M., Dall'ara, E., 2017. Effect of integration time on the morphometric, densitometric and mechanical properties of the mouse tibia. J. Biomech. 65, 203–211.
Palanca, M., Bodey, A.J., Giorgi, M., Viceconti, M., Lacroix, D., Cristofolini, L., Dall'ara, E., 2017. Local displacement and strain uncertainties in different bone types by digital volume correlation of synchrotron microtomograms. J. Biomech. 58, 27–36.
Palanca, M., Tozzi, G., Cristofolini, L., Viceconti, M., Dall'ara, E., 2015. Three-dimensional local measurements of bone strain and displacement: comparison of three digital volume correlation approaches. J. Biomech. Eng. 137, 071006–1 − 071006-14.
Patel, T.K., Brodt, M.D., Silva, M.J., 2014. Experimental and finite element analysis of strains induced by axial tibial compression in young-adult and old female C57Bl/6 mice. J. Biomech. 47, 451–457.
Pereira, A.F., Javaheri, B., Pitsillides, A.A., Shefelbine, S.J., 2015. Predicting cortical bone adaptation to axial loading in the mouse tibia. J. R. Soc. Interface 12.
Pistoia, W., Van Rietbergen, B., Lochmüller, E.M., Lill, C.A., Eckstein, F., Rüegsegger, P., 2002. Estimation of distal radius failure load with micro-finite element analysis models based on three-dimensional peripheral quantitative computed tomography images. Bone 30, 842–848.
Razi, H., Birkhold, A.I., Zaslansky, P., Weinkamer, R., Duda, G.N., Willie, B.M., Checa, S., 2015. Skeletal maturity leads to a reduction in the strain magnitudes induced within the bone: a murine tibia study. Acta Biomater. 13, 301–310.
Roberts, B.C., Perilli, E., Reynolds, K.J., 2014. Application of the digital volume correlation technique for the measurement of displacement and strain fields in bone: a literature review. J. Biomech. 47, 923–934.
Schulte, F.A., Ruffoni, D., Lambers, F.M., Christen, D., Webster, D.J., Kuhn, G., Müller, R., 2013. Local mechanical stimuli regulate bone formation and resorption in mice at the tissue level. PLoS One 8 (e62172-e62172).
Schwiedrzik, J., Gross, T., Bina, M., Pretterklieber, M., Zysset, P., Pahr, D., 2016. Experimental validation of a nonlinear μFE model based on cohesive-frictional plasticity for trabecular bone. Int. J. Numer. Methods Biomed. Eng. 32 (e02739-n/a).
Stadelmann, V.A., Hocke, J., Verhelle, J., Forster, V., Merlini, F., Terrier, A., Pioletti, D.P., 2009. 3D strain map of axially loaded mouse tibia: a numerical analysis validated by experimental measurements. Comput. Methods Biomech. Biomed. Eng. 12, 95–100.
Sztefek, P., Vanleene, M., Olsson, R., Collinson, R., Pitsillides, A.A., Shefelbine, S., 2010. Using digital image correlation to determine bone surface strains during loading and after adaptation of the mouse tibia. J. Biomech. 43, 599–605.
Van Rietbergen, B., Weinans, H., Huiskes, R., Odgaard, A., 1995. A new method to determine trabecular bone elastic properties and loading using micromechanical finite-element models. J. Biomech. 28, 69–81.
Waarsing, J.H., Day, J.S., Van der linden, J.C., Ederveen, A.G., Spanjers, C., De clerck, N., Sasov, A., Verhaar, J.A.N., Weinans, H., 2004. Detecting and tracking local changes in the tibiae of individual rats: a novel method to analyse longitudinal in vivo micro-CT data. Bone 34, 163–169.
Webster, D.J., Morley, P.L., Van Lenthe, G.H., Müller, R., 2008. A novel in vivo mouse model for mechanically stimulated bone adaptation – a combined experimental and computational validation study. Comput. Methods Biomech. Biomed. Eng. 11, 435–441.
Wolfram, U., Wilke, H.-J., Zysset, P.K., 2010. Valid μ finite element models of vertebral trabecular bone can be obtained using tissue properties measured with nanoindentation under wet conditions. J. Biomech. 43, 1731–1737.
Yang, H., Butz, K.D., Duffy, D., Niebur, G.L., Nauman, E.A., Main, R.P., 2014. Characterization of cancellous and cortical bone strain in the in vivo mouse tibial loading model using microCT-based finite element analysis. Bone 66, 131–139.
Zauel, R., Yeni, Y.N., Bay, B.K., Dong, X.N., Fyhrie, D.P., 2005. Comparison of the linear finite element prediction of deformation and strain of human cancellous bone to 3D digital volume correlation measurements. J. Biomech. Eng. 128, 1–6.